

# Optomechanical Ramsey Interferometry

Kenan Qu<sup>1</sup>, Chunhua Dong<sup>2,3,\*</sup>, Hailin Wang<sup>4</sup>, and G. S. Agarwal<sup>1</sup>

<sup>1</sup>*Department of Physics, Oklahoma State University, Stillwater, Oklahoma, 74078, USA*

<sup>2</sup>*Key Laboratory of Quantum Information, University of Science and Technology of China, Hefei 230026, P. R. China*

<sup>3</sup>*Synergetic Innovation Center of Quantum Information and Quantum Physics, University of Science and Technology of China, Hefei, Anhui 230026, P. R. China. and*

<sup>4</sup>*Department of Physics, University of Oregon, Eugene, Oregon 97403, USA*

(Dated: August 25, 2014)

We adopt the Ramsey's method of separated oscillatory fields to study coherences of the mechanical system in an optomechanical resonator. The high resolution Ramsey fringes are observed in the emission optical field, when two pulses separated in time are applied. We develop a theory to describe the transient optomechanical behavior underlying the Ramsey fringes. We also perform the experimental demonstration using a silica microresonator. The method is versatile and can be adopted to different types of mechanical resonators, electromechanical resonators.

PACS numbers: 42.50.Wk, 07.10.Cm, 03.75.Dg

## I. INTRODUCTION

The Ramsey method [1–4] of separated oscillatory fields is a highly successful method of precision spectroscopy and has been extensively used in a wide spectral range starting from radio frequency to optical domain. This method has yielded the atomic and molecular transition frequencies with very high precision especially by using phase coherent pulses with a duration short compared to the atomic decay times. The Ramsey technique is an interference techniques in which one studies the result of the quantum mechanical amplitudes in different domains where fields are applied. The Ramsey's interferometric technique has so far been used in the context of the study of the phase coherence in atomic and molecular systems [5–7]. Ramsey method has been especially successful in the detection of quantum coherences, such as in the detection of the Cat states of the electromagnetic field [8–10]. In this paper, we present a demonstration of the Ramsey interferometry (RI) in the context of a macroscopic system like a nanomechanical system. The Ramsey interferometry is especially important in probing the dynamics of the nanomechanical system as the detected interference signals would be sensitive to any dynamical changes in the mechanical oscillator in the time between which the pulses are off. The dynamics is a direct measure of the coherence time of the mechanical mirror which is an important issue in precision measurements [11]. We note that a variety of coherent techniques have been used to study optomechanical and electromechanical systems. These techniques primarily make use of the electromagnetically induced transparency and absorption [12–16] and the resulting applications like storage of light [18], slow light [16], etc. We also note that in a recent work [17], Ramsey interferometry is used to probe the dynamical behavior of two nanostring resonators coupled by an rf field. These authors realized a two level

system in this manner and then applied the technique of Ramsey interferometry as originally developed by Ramsey. In our work we perform Ramsey interferometry using an optical mode and a mechanical mode.

In atomic systems, the RI uses two spatially or temporally separated laser pulses to interact with atoms and detects the excitation probability of the atoms. Each laser pulse drives the atomic transition between the ground state  $|g\rangle$  and excited state  $|e\rangle$ . The atomic transition probability after a single weak pulse excitation [2] has a form [2] of  $p_s = g^2\tau^2\text{sinc}^2(\Delta\tau/2)$ , where  $\Delta$  is the frequency detuning between the laser and the atomic transition frequency. For simplicity, we use square pulses although other pulse forms can be used. Ramsey's two-pulse scheme yields sharper interference patterns without requiring a long interaction time. It has the excitation probability  $p_R = p_s(\cos\Delta T + 1)$ . Here the pulse separation in time  $T$  is shorter than the decay time of the atoms. Note that we use weak pulses in contrast to the case where Rabi oscillations are used. The pattern arises from the quantum interference of two paths in which the atom can get excited. The RI is expected to be useful whenever we have a system with a long decay time. Therefore, we make use of the very long decay time of the mechanical coherence [18–20] to demonstrate Ramsey interferometry in an optomechanical system (OMS).

There are similarities between this work and the storage work [18]. In storage work, one demonstrates the ability of the optomechanical system to store light pulses and to recover these. In RI, the objective is quite different: Here one wants to have a sensitive probe of the dynamics of the mirror and even a sensitive probe of the displacements. Thus in storage, the focus is on optical pulses whereas in RI the focus is on the mechanical element.

The organization of this paper is as follows: In Sec. II, we describe in detail the experimental setup and method of RI in optomechanics; we also show the results exhibiting Ramsey interference patterns. In Sec. III, we theoretically explain the phenomenon starting from the Hamil-

\* chunhua@ustc.edu.cn

tonian and obtain the condition to see Ramsey pattern in optomechanics. In Sec. VI we present our conclusions. Since our experiment is done with fields in the classical domain, we obtain theoretical results valid in this regime only.

## II. EXPERIMENT AND RESULT

In this article, we consider a generic OMS which contains a Fabry-Perot optical cavity with an oscillating mirror on one side, as in Fig. 1a. The motion of this mirror is driven by the radiation pressure force of the optical mode. This model is applicable to a large number of other systems, such as electromechanical systems [21], Brillouin modes in microfluidic devices [22], and mechanical breathing modes in silica microspheres [18], microtoroids [19], or microdisks [20]. For the proposed optomechanical RI, we enable the optomechanical coupling in two time-separated regions, during which a pair of laser pulses including both driving pulse and probe pulse are sent into the cavity (see Fig. 1a). The probe laser, with frequency  $\omega_p$ , is near the cavity resonance,  $\omega_c$  and the driving laser, with frequency  $\omega_l$ , is near the red sideband of the cavity resonance,  $\omega_c - \omega_m$ , with  $\omega_m$  being the mechanical frequency (see Fig. 1b). For convenience, we also define two frequency parameters  $x = \Delta - \omega_p + \omega_l$ ,  $y = \omega_m - \omega_p + \omega_l$ . Note that  $x \approx \omega_c - \omega_p$  and is close to zero if the probe field is on resonance with the cavity frequency. Then  $y \sim 0$  if  $\omega_l \sim \omega_c - \omega_m$ . The pulse sequence is shown in Fig. 1(c), where we denote the widths of the pulses by  $\tau_1$  and  $\tau_2$  and the separation by  $T$ . The time-dependent amplitudes of the driving and probe,  $\mathcal{E}_l(t)$  and  $\mathcal{E}_p(t)$ , are both nonzero only during the pulses:  $\mathcal{E}_l(t) = \mathcal{E}_l$  and  $\mathcal{E}_p(t) = \mathcal{E}_p$  for  $t \in [0, \tau_1] \cup [T + \tau_1, T + \tau_1 + \tau_2]$ , and  $\mathcal{E}_l(t) = \mathcal{E}_p(t) = 0$  otherwise.

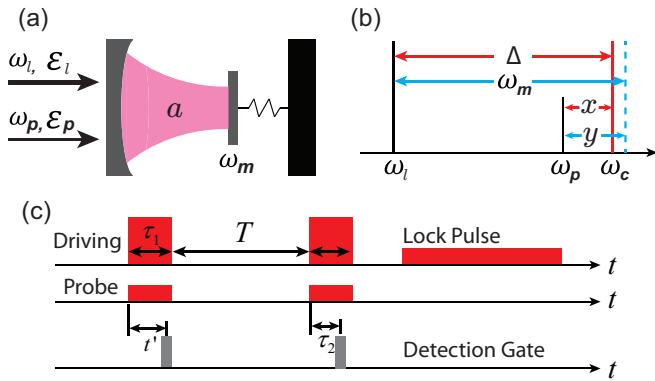


FIG. 1. (a) Sketch of the OMS. (b) The frequency relations of different modes in OMS. The labellings are explained in the text. (c) Sketch of the Ramsey pulses sequence applied to OMS.

In a RI setup, two pairs of pulses with separation  $T$  are sent to the cavity. Two processes are taking place when a pulse pair is in the cavity: ① the coupling and

probe photons combine and produce coherent phonons; and ② the coherent phonons combine with the coupling photons and generate an anti-Stokes sideband near the cavity resonance. The application of the first pulse pair creates both coherent phonons and cavity photons. After the first pulse pair, the optical mode decays rapidly during the free evolution and it becomes negligible as  $e^{-(\kappa/2)T} \sim 0$ , where  $\kappa$  is the total decay rate of the cavity mode. On the other hand, the mechanical mode shows almost no decay as  $e^{-(\gamma_m/2)T} \approx 1$ , where  $\gamma_m$  is the mechanical damping rate. This is because  $\gamma_m \ll \kappa$ . Thus, before the second pulse pair is applied, the mechanical mode barely decays but gathers a phase  $\omega_m T$ . Now we examine the two paths which lead to the interference in the optical field produced at  $\omega_p$ . The phonon created in the zone “ $\tau_1$ ” survives and interacts with the driving laser to produce a photon at  $\omega_p$  via process ② in the zone “ $\tau_2$ ”. This is marked as path (i) in Fig. 2. Photons at  $\omega_p$  can also be generated entirely in the zone “ $\tau_2$ ”, as discussed earlier [path (ii) of Fig. 2]. These two paths are displayed in Fig. 2b and their coherent character leads to Ramsey fringes in the optical output field, which can be detected directly through heterodyne interference [24] with a local oscillator. Note that the pattern does not

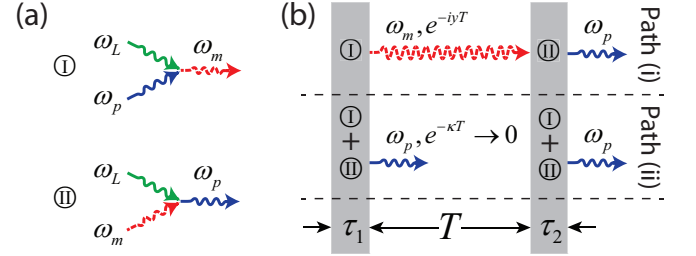


FIG. 2. The physical process of the photons and phonons in the Ramsey setup. The solid arrows refer to photons and dashed ones refer to phonons. (a) the driving photon combining a probe photon generates a phonon and the driving photon combining a phonon generates a probe photon. (b) the two paths of generating a photon at  $\omega_p$  and  $y = \omega_l + \omega_m - \omega_p$ .

arise from the direct interference of the two input probe pulses, since the free evolution time is much longer than the optical decay time,  $T \gg 1/\kappa$ . The mechanical oscillation is the only medium that can carry coherence during both pulses. Therefore, the fringes arise from the mechanical coherence effects although we observe such coherences in the optical fields. In the optomechanical RI, we take advantage of the long life time of the phonons in the mechanical resonator, as demonstrated in the previous optical pulse storage and retrieval works [18].

For the experimental demonstration, optical fields in a whispering gallery mode (WGM) of a silica microsphere ( $\kappa/2\pi \sim 30\text{MHz}$ ) with a diameter of  $33\mu\text{m}$  were coupled to the (1, 2) radial-breathing mechanical mode ( $\omega_m/2\pi \sim 94\text{MHz}$ ,  $\gamma_m/2\pi \sim 20\text{kHz}$  and  $Q \sim 1.3 \times 10^7$ ) of the microsphere. The WGM was excited through the evanescent field of a tapered optical fiber. Both the silica

microsphere and the tapered fiber were held in a clean room environment in order to avoid degradation of optical Q factors. In Figure 3(b-c), we show the WGM transmission resonance used in our experiment and the displacement power spectrum of the (1, 2) radial breathing mode of the microsphere [23]. A combination of acoustic-optic modulator (AOM) and electro-optic modulators (EOMs) were used to generate optical pulses with the desired duration, timing, and frequencies, as shown in Fig.3 (a). The driving and the locking pulses came from a single-frequency tunable diode laser (Toptica DLPRO 780) with  $\lambda \sim 780$  nm and with its frequency locked to the red sideband of a given WGM resonance using the Pound-Drever-Hall technique. The signal pulses were driven from the blue sideband generated by passing the driving pulses through EOM<sub>0</sub>. For the experimental results reported here, both the driving and the probe pulses were square shaped, with the same timing and with duration of  $4\mu\text{s}$ . Heterodyne detection was used for the measurement of the optical emission from the microsphere near the WGM resonance, with the driving laser pulse serving as the local oscillator [18]. A gated detection scheme was also used with a gate duration of  $1\mu\text{s}$ . The timing of the gate (see grey area in Fig.1c) determines the effective duration,  $\tau_2$ , of the second pulse pair involved in the RI.

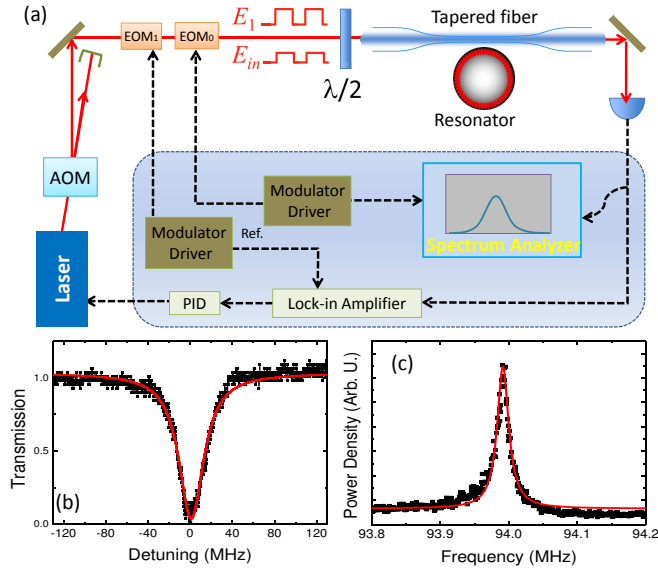


FIG. 3. (a) Schematic of the experimental setup for the Ramsey Interferometry, with solid lines representing the optical paths and dashed lines representing the electrical connections. (b) Transmission resonance for the WGM at  $\sim 780$ nm. (c) Displacement power spectrum of the (1, 2) radial breathing mode, obtained from the same sample. The solid red lines show a Lorentzian fitting.

Figures 4 show the heterodyne detected probe intensity as a function of the detuning between the probe and driving laser obtained with different durations  $\tau_2$ . The separation time,  $T$ , between the first and second pulse pairs is

set to  $4\mu\text{s}$  in the left column and  $8\mu\text{s}$  in the right column. The distinct spectral oscillations observed in these experiments demonstrate the Ramsey fringes for the OMS. As a reference, we also show in Figs. 4a and 4b the experimental results (solid circles) obtained in the absence of the second pulse pair. Experimentally, these were obtained with the detection gate positioned within the duration of the first pulse pair, as indicated in Fig. 1c. The spectral dip observed in this case arises from the *transient* optomechanically induced transparency (OMIT) [12–14].

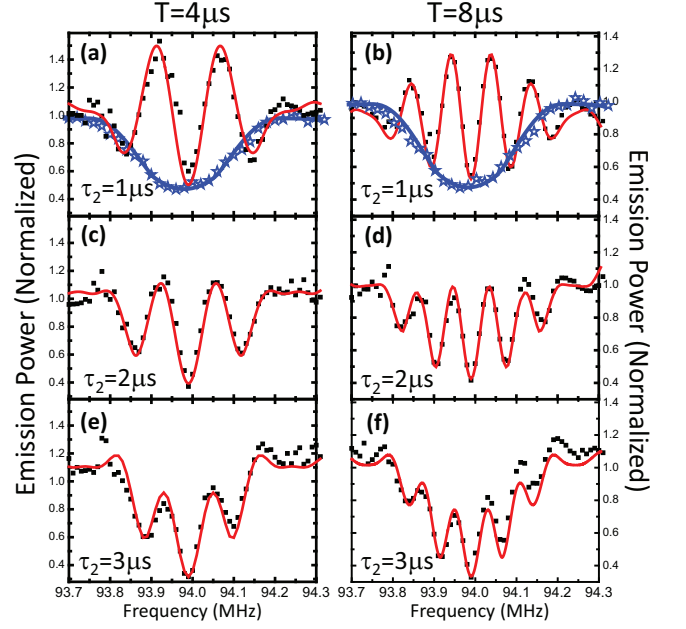


FIG. 4. Heterodyne detected probe intensity as a function of the detuning between the probe and driving lasers. The blue dots in (a) and (b) are obtained with the detection gate positioned within the first pulse pair with the delay time  $t' = 3\mu\text{s}$ . The black dots in (a-f) are obtained with the detection gate positioned within the second pulse pair with  $T$  and  $\tau_2$  indicated in the figure. The incident driving power used is  $3.4\text{mW}$ . The solid lines are results of theoretical calculations discussed in Sec. III.

### III. THEORETICAL MODEL

For a detailed theoretical analysis of optomechanical Ramsey fringes and for a direct comparison between experiment and theory, we use the optomechanical Hamiltonian written as [11, 25]

$$H = \hbar(\omega_c - \omega_l)a^\dagger a + \hbar\omega_m b^\dagger b - \hbar g a^\dagger a (b^\dagger + b) + i\hbar\mathcal{E}_l(t)(a^\dagger - a) + i\hbar[\mathcal{E}_p(t)a^\dagger e^{-i(\omega_p - \omega_l)t} + \text{c.c.}], \quad (1)$$

where we denote the optical and mechanical modes using annihilation operators  $a$  and  $b$ , respectively. The first line

in Eq. 1 contains the terms of the optical and mechanical unperturbed Hamiltonian and the interaction between them; and the terms in the second line describe interaction with the driving laser and the probe laser. The linear coupling rate  $g$  is given by  $(\omega_c/L)\sqrt{\hbar/(m\omega_m)}$  with  $L$  being the cavity length and  $m$  being the effective mechanical mass. The total decay rate of the cavity field includes the intrinsic decay rate  $\kappa_i$ , the rate at which the optical energy losses to the environment, and the external decay rate  $\kappa_e$  which is the loss rate associated with the waveguide-resonator interface. The driving and probe laser amplitudes are related to their powers  $\mathcal{P}_i$  by  $\mathcal{E}_i = \sqrt{\kappa\mathcal{P}_i/(\hbar\omega_i)}$ . We assume that the coupling laser is much stronger than the probe laser,  $\mathcal{E}_l \gg \mathcal{E}_p$ .

We follow the standard procedure to solve the problem by expanding the mean values of equations to the first order in  $\mathcal{E}_p$  using  $a = \alpha_0 + \alpha e^{-i(\omega_p - \omega_l)t}$  and  $b = \beta_0 + \beta e^{-i(\omega_p - \omega_l)t}$ , and get  $\alpha_0(t) = \frac{\mathcal{E}_l(t)}{\kappa/2 + i\Delta}$ ,  $\beta_0(t) = \frac{g}{\omega_m - i\gamma_m/2} |\alpha_0|^2$  with  $\Delta = \omega_c - \omega_l - 2|\alpha_0|^2 g^2 / \omega_m$  representing the effective detuning between the cavity and the driving field frequencies. The driving-enhanced coupling rate  $G(t) = |\alpha(t)|g$  is solely controlled by the coupling laser amplitude and we denote  $G(t) = G$  during the pulses and  $G(t) = 0$  otherwise. In the equations for the first order amplitudes  $\alpha$  and  $\beta$ , we make the rotating-wave approximation by eliminating the non-resonant fast oscillating terms  $e^{-2i(\omega_p - \omega_l)t}$  and  $e^{2i(\omega_p - \omega_l)t}$ . Physically, we ignore the terms corresponding to the processes of creating or eliminating both a photon and a phonon simultaneously. The simplified equations for the amplitudes  $\alpha$  and  $\beta$  are given by

$$\begin{aligned}\dot{\alpha} &= -ix\alpha - G(t)\beta - (\kappa/2)\alpha + \mathcal{E}_p(t), \\ \dot{\beta} &= -iy\beta + G(t)\alpha - (\gamma_m/2)\beta.\end{aligned}\quad (2)$$

The output optical field at frequency  $\omega_p$  at any time  $t$  can be derived from the input-output relation  $\mathcal{E}_o(t) = \kappa_e \alpha(t) - \mathcal{E}_p(t)$ . In our study, we work in the critical coupling regime with the internal and external coupling rates equal, i.e.  $\kappa_e = \kappa_i = \kappa/2$ . The  $\kappa$  gives the linewidth of the transmission around the WGM which for the data of Fig. 2 is  $2\pi \times 30\text{MHz}$ . We do heterodyne detection to get the intracavity field  $\kappa_e \alpha(t) = \mathcal{E}_o(t) + \mathcal{E}_p(t)$ .

We now study the mechanical field  $\beta_R$  and optical field  $\alpha_R$  after application of the two separated pulses. We give the approximate expressions which are normalized to  $\mathcal{E}_p$  by solving Eqs.(2):

$$\begin{aligned}\kappa_e \beta_R &\approx G \left[ \frac{e^{-(iy+\Gamma)\tau_1} - 1}{iy + \Gamma} e^{-i\phi - \mu} + \frac{e^{-(iy+\Gamma)\tau_2} - 1}{iy + \Gamma} \right] \mathcal{E}_p, \\ \kappa_e \alpha_R &\approx (2G\beta_R + 1)\mathcal{E}_p, \\ \phi &= y(\tau_2 + T), \quad \mu = \left(\frac{\gamma_m}{2}T + \Gamma\tau_2\right), \quad y = \omega_l + \omega_m - \omega_p,\end{aligned}\quad (3)$$

where  $\Gamma = 2G^2/\kappa + \gamma_m/2$  is the photon-phonon transfer rate in OMS and  $\phi$  denotes the accumulated phase which leads to the Ramsey fringes. The parameter  $\mu$  describes the decay of the signal, which causes the loss of visibility

in the Ramsey fringes. The two terms in  $\mu$  are corresponding to the mechanical decay in the free evolution time  $T$  and in the optomechanical interaction during the second pulse  $\tau_2$ .

We start by analyzing the mechanical mode given in Eq.(3). It contains two terms with the same form, each of which describes the phonon excitation due to the optomechanical interaction when the corresponding pulse  $\tau_i$  ( $i = 1, 2$ ) is on. However, there is a phase factor  $e^{-i\phi}$  multiplied to the first term. As  $\phi$  changes, the two terms in Eq.(3) either interfere constructively or destructively leading to the Ramsey fringes. The phase  $\phi = y(T + \tau_2)$ , i.e. the product of the frequency detuning and the evolution time, determines the fringe period. Note that the fringe period also depends on the parameter  $\Gamma$ . The period is exactly  $2\pi/(T + \tau_2)$  only when  $\Gamma = 0$  and it gets lower when  $\Gamma$  increases. The fringes get sharper as one increases  $T + \tau_2$ . However, a longer  $\tau_2$  can result in a decay of the signal, which can be seen from the parameter  $\mu = \Gamma\tau_2 + \frac{\gamma_m}{2}T$ . Considering  $\Gamma > \gamma_m$ , one should reasonably choose  $\tau_2 < 1/\Gamma$ . The numerator of each term  $e^{-(iy+\Gamma)\tau_i} - 1 \sim 0$  for a short  $\tau_i$ , and it increases along with  $\tau_i$ . This justifies that the phonon excitation is only prominent when  $\tau_i$  is large, which sets the characteristic time of phonon excitation in OMS, i.e.  $\Gamma\tau_i > 1$ . The electromagnetically induced transparency (EIT) occurs when  $\Gamma\tau_i \gg 1$ . In the optomechanical RI, a large  $\tau_1$  enhances the Ramsey fringes contrast, although the fringes can still be seen at a shorter  $\tau_1$ . Therefore, the conditions for the Ramsey fringes are  $\tau_1\Gamma \gtrsim 1$ ,  $\tau_2\Gamma < 1$ , and  $T\gamma_m \ll 1$ .

The optical field expressed in Eqs.(3) exhibits the same interference fringes as in the mechanical mode. This is important as the measurement of the output optical field becomes a direct probe of the Ramsey fringes in the mechanical system. For a direct comparison with the experiments, over a wide range of parameters we show the results of the theoretical calculations as solid curves in Fig. 4. The parameters used include  $\kappa/2\pi = 30\text{MHz}$ ,  $G/2\pi = 0.58\text{MHz}$ ,  $\gamma_m/2\pi = 20\text{kHz}$ , and the corresponding characteristic time  $1/\Gamma = 4.9\mu\text{s}$ . As shown in Fig. 4, the spectral position of the central Ramsey fringe overlaps exactly with the center of the OMIT dip and does not depend on either  $T$  or  $\tau_2$ . More importantly, the Ramsey fringes exhibit a period that is much smaller than the linewidth of the OMIT dip. In (a) with  $T = 4\mu\text{s}$  and  $\tau_2 = 1\mu\text{s}$ , the Ramsey fringe period is  $160\text{kHz}$ . As  $T + \tau_2$  increase from  $5\mu\text{s}$  in (a) to  $11\mu\text{s}$  in (f), the fringe period decreases from  $\sim 160\text{kHz}$  to  $\sim 80\text{kHz}$ . Overall, there is an excellent agreement between the theory (curves) and experiment (dots). The visibility of the Ramsey fringes is primarily determined by  $\tau_2$ . Fig. 4. reveals the loss of fringe visibility with increasing  $\tau_2$ . We note that for comparison with the experiments, we use directly Eqs.(2). It is only for understanding the physical behavior we used approximate Eqs.(3)

In order to appreciate the versatility of the Ramsey fringes in OMS, we show in Fig. 5 additional results of



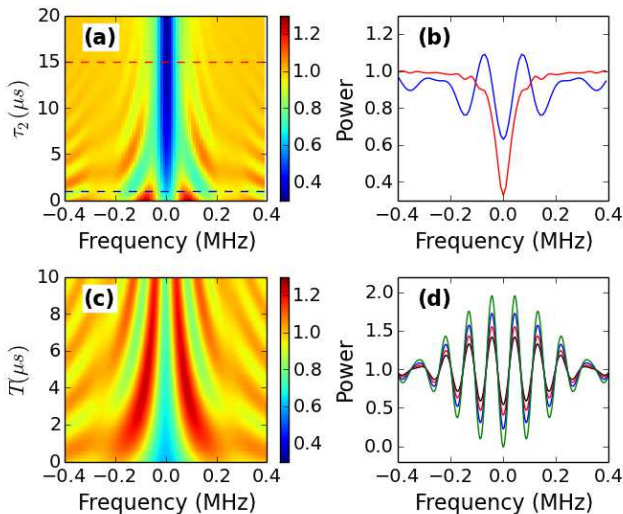


FIG. 5. (a) Simulation as a function of  $\tau_2$  with fixed  $\tau_1 = 4\mu\text{s}$ ,  $T = 4\mu\text{s}$ ,  $\kappa/2\pi = 30\text{MHz}$ ,  $G/2\pi = 0.58\text{MHz}$ ,  $\gamma_m/2\pi = 20\text{kHz}$ . (b) The spectra with  $\tau_2 = 1\mu\text{s}$  (blue curve) and  $\tau_2 = 15\mu\text{s}$  (red curve), as dashed line shown in (a). (c) The Ramsey fringe with different delay time  $T$ . Other parameters are same as (a) except  $\tau_2 = 0.1\mu\text{s}$ . (d) The Ramsey fringes with  $T = 10\mu\text{s}$  and different  $\gamma_m/2\pi = 10, 20, 30, 40\text{kHz}$  for green, blue, red and black curves, respectively. Other parameters are same as in (c).

simulations under a range of parameters. As shown in Fig. 5a, the interference fringes decrease with the longer  $\tau_2$ , which means no coherent phonons for interference. This is due to the decay term  $\mu$  in Eq.(3). As noted there we need  $\Gamma\tau_2$  to be small. In Fig. 5b we can see that, when  $\tau_2$  is short, the spectrum shows interference; but with the long enough  $\tau_2$ , the fringes in the spectrum cannot be seen and the spectrum reduces to a steady-state result. With other parameters fixed, the increase in time  $T$  leads to a decreasing in the Ramsey fringe period.

However, after long enough time, the Ramsey fringes disappear because of the damping of phonons, as shown in Fig. 5c. Therefore, we should choose the  $\gamma_m$  as small as possible during the experiment for observing Ramsey fringes. This is demonstrated more clearly in Fig. 5d, which shows the visibility of the Ramsey fringes with different  $\gamma_m$ .

#### IV. CONCLUSION

In conclusion we have demonstrated how the high resolution Ramsey method of separated oscillatory fields can be adopted to study coherences in a macroscopic system like a nanomechanical oscillator. We have presented the underlying theory and the experimental demonstration using silica microresonators. The method is quite versatile and can be adopted to different types of mechanical resonators and electromechanical resonators. More complex applications can include the study of the dynamical interaction between the mechanical oscillators. Future work may also include the demonstration of the Ramsey fringes using excitations at the single photon level which would imply excitation of a mechanical oscillator at the single phonon level needless to say that achieving quantum regime experimentally would require at least the coherent fields at the single photon level as well as cooling to temperatures such that the mean phonon number is less than 1. The Ramsey method is also expected to be useful in producing time-bin entanglement involving a phonon and a photon.

K.Q. and C.H.D. contributed equally to this work. C.H.D. was supported by the National Basic Research Program of China (Grant No.2011CB921200), the Knowledge Innovation Project of Chinese Academy of Sciences (Grant No.60921091), the National Natural Science Foundation of China (Grant No.61308079), the Fundamental Research Funds for the Central Universities. H.W. acknowledges support from NSF under grant No. 1205544.

- 
- [1] N. F. Ramsey, Phys. Rev. **78**, 695 (1950).
  - [2] M. Salour, Rev. Mod. Phys. **50**, 667 (1978).
  - [3] Ye. V. Baklanov, B. Ya. Dubetskii and V. P. Chebotayev, Appl. Phys. **11**, 201 (1976).
  - [4] M. M. Salour and C. Cohen-Tannoudji, Phys. Rev. Lett. **38**, 757 (1977).
  - [5] D. J. Wineland, J. J. Bollinger, W. M. Itano, F. L. Moore, and D. J. Heinzen, Phys. Rev. A **46**, R6797 (1992).
  - [6] D. Leibfried, M. D. Barrett, T. Schaetz, J. Britton, J. Chiaverini, W.M. Itano, J.D. Jost, C. Langer, and D. J. Wineland, Science **304**, 1476 (2004).
  - [7] S. Cavalieri, R. Eramo, M. Materazzi, C. Corsi, and M. Bellini, Phys. Rev. Lett. **89**, 133002 (2002).
  - [8] S. Haroche and J.-M. Raimond, Exploring the Quantum: Atoms, Cavities and Photons (Oxford University Press, New York, 2006).
  - [9] M. Brune, E. Hagley, J. Dreyer, X. Maître, A. Maali, C. Wunderlich, J. M. Raimond, and S. Haroche, Phys. Rev. Lett. **77**, 4887 (1996).
  - [10] J.-M. Raimond, M. Brune, and S. Haroche, Rev. Mod. Phys. **73**, 565 (2001).
  - [11] M. Aspelmeyer, T. J. Kippenberg, and F. Marquardt, arXiv:1303.0733 (2013).
  - [12] G. S. Agarwal and S. Huang, Phys. Rev. A **81**, 041803(R) (2010).
  - [13] S. Weis, et al., Science **330**, 1520 (2010); J. D. Teufel, et al., Nature (London), **471**, 204 (2011).
  - [14] Y. Liu, M. Davanço, V. Aksyuk, and K. Srinivasan, Phys. Rev. Lett. **110**, 223603 (2013).
  - [15] Kenan Qu and G. S. Agarwal, Phys. Rev. A **87**, 031802

- (2013).
- [16] A. H. Safavi-Naeini, T. P. M. Alegre, J. Chan, M. Eichenfield, M. Winger, Q. Lin, J. T. Hill, D. E. Chang, and O. Painter, *Nature (London)*, **472**, 69 (2011).
  - [17] T. Faust, J. Rieger, M. J. Seitner, J. P. Kotthaus and E. M. Weig, *Nature Physics* **9**, 485 (2013).
  - [18] V. Fiore, Y. Yang, M. C. Kuzyk, R. Barbour, L. Tian, and H. Wang, *Phys. Rev. Lett.* **107**, 133601 (2011); C. Dong, V. Fiore, M. C. Kuzyk, and H. Wang, *Phys. Rev. A* **87**, 055802 (2013); V. Fiore, C. Dong, M. C. Kuzyk, and H. Wang, *Phys. Rev. A* **87**, 023812 (2013).
  - [19] H. Lee, T. Chen, J. Li, K. Y. Yang, S. Jeon, O. Painter and K. J. Vahala, *Nature Photonics* **6**, 369 (2012).
  - [20] I. Favero and K. Karrai, *Nature Photonics* **3**, 201-205 (2009).
  - [21] F. Massel, S. U. Cho, J.-M. Pirkkalainen, P. J. Hakonen, T. T. Heikkilä, and M. A. Sillanpää. *Nat. Commun.* **3**, 987 (2012).
  - [22] G. Bahl, K. H. Kim, W. Lee, J. Liu, X. Fan, and T. Carmon, *Nat. Commun.* **4**, 1994 (2013).
  - [23] Y.-S. Park and H. Wang, *Nature Physics* **5**, 489 (2009).
  - [24] G. S. Agarwal, “Quantum Optics”, (Cambridge University Press, 2012), Sec.13.4.
  - [25] C. Genes, A. Mari, D. Vitali, and P. Tombesi, *Adv. At., Mol. Opt. Phys.* **57**, 33 (2009).